# Low lying electronic states of rare gas–oxide anions: Photoelectron spectroscopy of complexes of $O^-$ with Ar, Kr, Xe, and $N_2$

Helen L. de Clercq,[a] Jay H. Hendricks,[b] and Kit H. Bowen[c]
*Department of Chemistry, The Johns Hopkins University, Baltimore, Maryland 21218*

(Received 26 November 2001; accepted 15 May 2002)

The negative ion photoelectron spectra of the oxide anion complexes $O^-Rg$, Rg=Ar, Kr, and Xe, and $O^-N_2$ have been recorded. In each spectrum, two partially resolved peaks were observed, their relative intensities varying with source conditions. These peaks were assigned to photodetachment transitions from the $^2\Sigma$ ground state and unresolved $^2\Pi_{3/2,1/2}$ low-lying excited states of the anion. From our data we find dissociation energies and bond lengths for the $^2\Sigma$ and $^2\Pi$ anion states. Periodic trends in the bond length and dissociation energy are examined and compared to those in the isoelectronic neutral halogen rare gas systems and the effect of anisotropy in the interatomic potential and relative interaction strength is examined. From our data we find that the dissociation energies in the anion system are much larger but that the $^2\Sigma$-$^2\Pi$ splitting is significantly lower. In addition to the diatomic clusters, we report the photoelectron spectra of the $O^-Kr_{n=2-5}$ and $O^-Xe_{n=2-3}$ clusters and tabulate the vertical detachment energies and peak widths. From a comparison of the energetics and peak broadening we are able to make a determination of the general structure of the $n=2$ and $n=3$ clusters. © *2002 American Institute of Physics.*
[DOI: 10.1063/1.1491410]

## I. INTRODUCTION

The weak interaction between closed shell neutral species has been investigated extensively over the past decades. These efforts have produced a large body of experimental and theoretical literature extending from the relatively simple interatomic to atom–molecule, intermolecular, and multibody systems. The nature of the weak interaction between open and closed shell species lies between that of a nonbonding closed shell interaction and the covalent bonding of open shell atoms or radicals. Compared to the current high level of understanding for closed shell systems, investigations of open shell complexes are still in an early stage of development. This is partly due to the experimental difficulties in generating stable molecular beams of atomic and molecular radicals in sufficient intensity as well as the theoretical complexities involved. Nonetheless, significant strides have been made in a number of areas, in particular metal atom,[1] halogen atom, and small molecular radical[2] rare gas complexes. An additional example of a weak interaction that is stronger than van der Waals is that between ions and neutrals. The photodetachment of halogen anion rare gas complexes undertaken by Neumark and co-workers neatly encompasses both of these systems. In a series of zero electron kinetic energy (ZEKE) spectroscopy studies these investigators have found spectroscopic constants for the closed shell anion and the corresponding open shell neutral states for rare gas diatomic complexes of $Cl^-$, $Br^-$, and $I^-$.[3–6] Larger argon clusters of $Br^-$ and $I^-$, and xenon clusters of $I^-$, have also been examined by ZEKE and partially discriminated threshold photodetachment experiments.[7,8] The ion-induced dipole interaction in closed shell ion-neutral complexes is stronger than van der Waals but, like the van der Waals interaction, is nonbonding. Here we present the 488 nm negative ion photoelectron spectra of dimers of the type $O^-Rg$, where Rg is a $^1S_0$ rare gas atom or nonreactive $^1\Sigma_0$ molecule. The interaction in this case is between an open shell anion and a closed shell neutral and represents a further step in interaction strength for weakly bound systems. The most apparent difference between open and closed shell systems (whether ion or neutral) is that open shell systems have spin and in many cases orbital angular momentum. The implications for anion complexes are unique in that while closed shell anions do not generally support stable excited electronic states, open shell anions may have spin orbit states that lie below the ground state neutral potential. For example, the electron affinity (EA) of the oxygen atom is 1.461 eV and the spin-orbit splitting between the $O^-$ $^2P_{3/2,1/2}$ states is only 21.961 meV.[9–11] In addition to spin orbit splitting, the spatial degeneracy of $m_l$ levels in the open shell species is removed upon interaction with the closed shell partner. Hence, additional low-lying states are produced due to the anisotropy of the interaction. Relative peak intensities in the photodetachment of open shell anions will therefore depend upon the thermal population of low-lying excited anion states as well as the branching ratios for the respective anion→neutral photodetachment transitions. In the case of the atomic oxygen anion, photodetachment of $2p$ valence electrons results in six closely spaced transitions between the $O^-(^2P_{3/2,1/2})$ anion, and the $O(^3P_{2,1,0})$ neutral states. The branching ratios for these six transitions at 488.0 and 514.5 nm, as well as the $O^-$

[a]Present address: Department of Chemistry, Howard University, Washington, DC 20059.
[b]Present address: National Institute of Standards and Technology, Gaithersburg, MD.
[c]Author to whom correspondence should be addressed. Electronic mail: kitbowen@jhunix.hcf.jhu.edu

 

spin orbit splitting, have been well characterized by Hotop and co-workers.[9] Subsequent threshold detachment by Lineberger and co-workers determined the $O^-$ spin orbit splitting to greater precision, and is currently the most accurate value for this quantity.[10] In $O^-Rg$ complexes, collinear and perpendicular orientations of the singly occupied oxygen anion $2p$ orbital produce two electronic states, $\Sigma$ and $\Pi$ in Hund's case *a* representation. This representation is justified in the oxygen anion complexes by the small $O^-$ spin orbit splitting relative to the ion-induced dipole electrostatic interaction and is discussed in the interpretation section. The $\Sigma$ state minimizes electron–electron repulsion and is the ground state of $O^-Rg$. With both orientation and spin orbit effects taken into account, the interaction of the $O^-(^2P_{3/2,1/2})$ atomic anion with a rare gas atom results in three electronic states, the $^2\Sigma_{1/2}$ ground state and low-lying $^2\Pi_{3/2,1/2}$ excited states. The $^2\Sigma_{1/2}$ and $^2\Pi_{3/2}$ state dissociate to the $O^-(^2P_{3/2})+Rg$ asymptote. The $^2\Pi_{1/2}$ state dissociates to the $O^-(^2P_{3/2})+Rg$ asymptote. In a like manner, the three spin orbit states of the $O(^3P_{2,1,0})$ atom lead to six states in the neutral oxygen rare gas complex. Hence, 488 nm photodetachment of $O^-Rg$ accesses 18 photodetachment transitions between states associated with the $O^-(^2P_{3/2,1/2})+Rg$ and $O(^3P_{2,1,0})+Rg$ asymptotes. (Detachment to neutral oxygen $^1S$ and $^1D$ states is well outside of the 488 nm photon range.)

First observed in 1946, the characteristic green emission in discharges in mixtures of $O_2$ and xenon[12] was determined to be oxygen $^1S\rightarrow{}^1D$ emission perturbed by association with rare gas.[13] Subsequent interest in excimer lasing in the 1970s motivated many of the experimental studies of the neutral oxygen–rare gas systems,[14–18] and since that time, the potential curves of the neutral oxygen–rare gas complexes have been studied theoretically by a number of investigators.[19–21] Examination of the ground state $O(^3P)+Rg(^1S)$ potential curves was important to this effort because quenching of $O(^1D)$ to the $O(^3P)$ ground state by collision with rare gas depletes the lower laser level.[22] As a consequence, these investigators were most interested in the short-range repulsive part of the $O(^3P)+Rg(^1S)$ potential, where curve crossing with the $O(^1D)+Rg(^1S)$ potential occurs, and neglected or treated lightly the van der Waals interaction.

More recently the $O(^3P)+Rg(^1S)$ potential has been explored in detail by Aquilanti and co-workers[23] as part of their efforts in examining the anisotropy of the interaction between open shell atoms and rare gas atoms and nonreactive molecules.[24–29] In these experiments, absolute integral cross sections were measured as a function of beam velocity for the scattering of open shell atoms with rare gases or nonreactive closed shell molecules. These results were analyzed to express the electrostatic interaction as a spherical, $V_0$, and anisotropic, $V_2$, component. These are related to the $\Sigma$ and $\Pi$ potentials by simple linear combinations $V_0=1/3(V_\Sigma+2V_\Pi)$ and $V_2=5/3(V_\Sigma-V_\Pi)$. Morse parameters for the spherical part of the interaction were determined from the glory pattern. Parameters for the anisotropic interaction were found from the overall behavior of the cross sections as well as dampening of the glory amplitudes. This method describes most accurately the van der Waals portion of the potential, finding well shape, depth, and equilibrium radius. In this manner the six lowest states of the rare gas oxides associated with the $O(^3P_{2,1,0})+Rg(^1S_0)$ asymptotes for Rg = He, Ne, Ar, Kr, and Xe[23] were characterized. A subsequent study found this information for the oxide complexes of $H_2$ and $CH_4$.[25] With the neutral states well characterized, negative ion photoelectron spectroscopy is able to provide information on the energetics of the anion complex.

The only prior experimental information for oxide anion rare gas complexes is from ion mobility studies of $O^-He$[30,31] and a photoelectron study of $O^-Ar_{n=1\text{-}26,34}$ performed by our group.[32] In addition to fits of the $O^-He$ ion mobility data,[33,34] an *ab initio* calculation of the $O^-Ar$ potential has been carried out by Sheehy.[35] These unpublished results provided welcomed theoretical guidance during the analysis of the experimental data reported here. Since then, an additional theoretical study of $O^-Ar$ has been performed by Chalasiński and co-workers, who successfully modeled the $O^-Ar$ photoelectron spectrum reported here using a combined *ab initio* atoms-in-molecule approach.[36] That work is summarized in their recent review.[37] These investigators shared with us their recent results for $O^-Kr$, which are discussed in their accompanying paper.[38]

In our experiment the oxide anion complexes, $O^-Rg$ (Rg= Ar, Kr, Xe, and $N_2$) were produced and photodetached. Their negative ion photoelectron spectra were recorded under varying source conditions and are shown in the results section. Each of the photoelectron spectra contain two detachment features whose relative intensity varied with source conditions. This indicates that the transitions are dependent upon the thermal population of excited states of the anion and the two peaks have been assigned to photodetachment from a $^2\Sigma_{1/2}$ anion ground state and unresolved $^2\Pi_{3/2,1/2}$ spin orbit excited states of the anion. The vertical detachment energies (VDEs) of the spectral features have been measured and the transitions involved are discussed in detail in the interpretation section. Using these data with the information on the corresponding neutral potentials of Aquilanti and co-workers,[23] dissociation energies of the anion complexes are calculated and compared to theory. With assistance from theoretical calculations of the $O^-Ar$ potential,[35] the bond lengths of the $O^-Kr$ and $O^-Xe$ complexes are estimated. In addition to the periodic trends that form the bulk of this examination, the photoelectron spectra of the cluster series $O^-Kr_{n=2-5}$ and $O^-Xe_{n=2-3}$ were also recorded. A consistent trend in peak broadening is observed over the Kr, Xe, and, the previously published, Ar clusters. The broadening trend will be discussed in light of the solvation energies measured with consideration of the possible packing structures for the additional rare gas solvent.

## II. EXPERIMENTAL METHOD

Negative ion photoelectron spectroscopy is conducted by crossing a fixed frequency laser with a mass selected beam of negative ions under field-free and collision-free conditions. The energy required to photodetach an electron is equal to the difference between the photon energy and the kinetic energy carried away by the departing electron. The beamline and photoelectron spectrometer used in this experiment have been described in detail previously.[39,40] Briefly, anions are

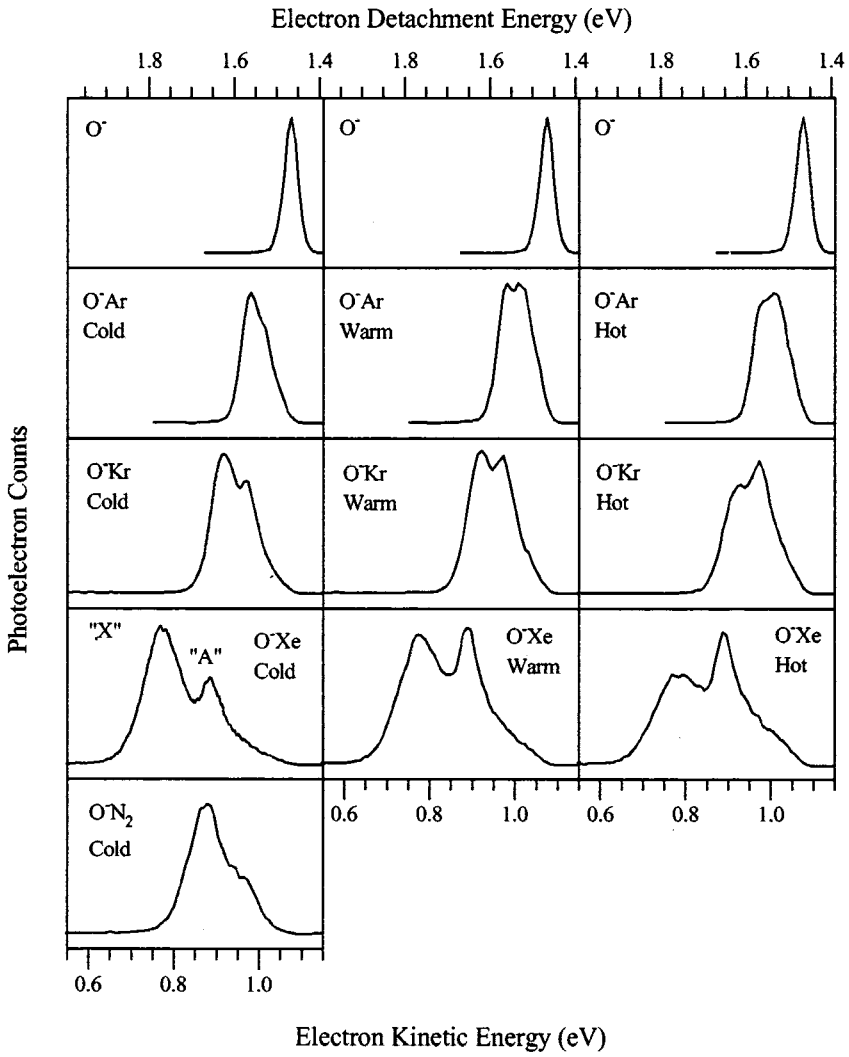


FIG. 1. Photoelectron spectra of $O^-Rg$, Rg=Ar, Kr, Xe, and $O^-N_2$ produced under expansion source conditions characterized generally as "hot, warm, and cold."

extracted from the ionized expansion of a supersonic source, accelerated to 500 eV, and mass selected by a Wien filter. The beam of mass selected negative ions is crossed with the 488 nm output of an intracavity argon ion laser. A small solid angle of detached electrons is collected into a hemispherical electron energy analyzer run at a constant 5 eV pass energy. The electron energy resolution of this spectrometer is 25 meV and was calibrated to the known EA of O.[10,11]

For these experiments the expansion source was run with a 12–17 $\mu$m diameter nozzle typically backed with 2–7 atm of argon (either seeded with 5%–10% Kr, Xe, $N_2$ or just neat). The stagnation chamber of the source was cooled to $\sim -70\,^{\circ}C$ by recirculating methanol through a cooling bath (usually dry ice and acetone) and then through the cooling jacket of the source. The background pressure ranged from $8\times10^{-5}$ to $1\times10^{-4}$ Torr in the source chamber. $N_2O$ was introduced near the expansion region through a small diameter copper "pick-up" line located 1–3 mm above the nozzle and 2 mm downstream. Some portion of $N_2O$ ionized in the plasma forming $O^-$ and $NO^-$ which clustered with the expansion gas. (Little clustering of $N_2O$ onto these sub-ions was observed even though $N_2O$ interacts more strongly with ions than any of the rare gases examined.[41]) We have found modest self-clustering of the pick-up gas to be characteristic of our pick-up source. This indicates that the pick-up gas is entrained in the expansion beyond the clustering region in front of the nozzle. The advantage of using the pick-up line in lieu of a seeded gas expansion is that one can prepare species in the jet that you could not otherwise make, either because the two gaseous feedstocks are reactive, because they would form competing cluster series, or because they would increase the beam and/or plasma electron temperature.

## III. RESULTS

The negative ion photoelectron spectra of $O^-Rg$ (Rg $=$Ar,Kr,Xe) and $O^-N_2$ were taken with source conditions characterized rather generally as hot, warm, and cold, and are presented in Fig. 1. The most noticeable feature about these spectra is the presence of two photodetachment peaks. Barely resolved in $O^-Ar$, the spacing between the peaks increases with the periodicity of the rare gas until they are quite distinct in $O^-Xe$. By varying source conditions, stagnation chamber temperature, backing pressure, and filament emission current and bias, we were able to alter the relative intensities of the peaks, indicating that they result from de-

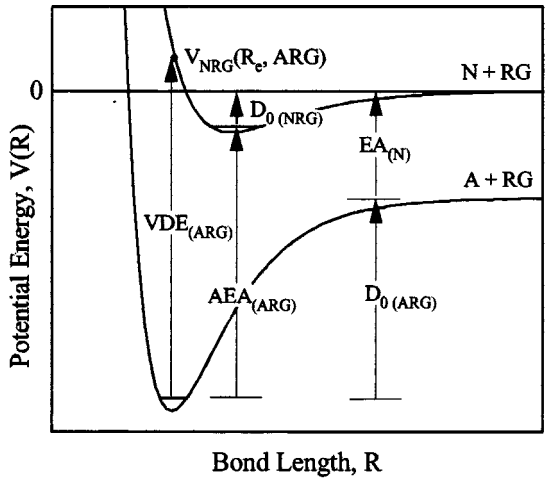


FIG. 2. Photodetachment relationships for transitions from a weakly bound anion rare gas complex to the corresponding neutral, ARg→NRg.

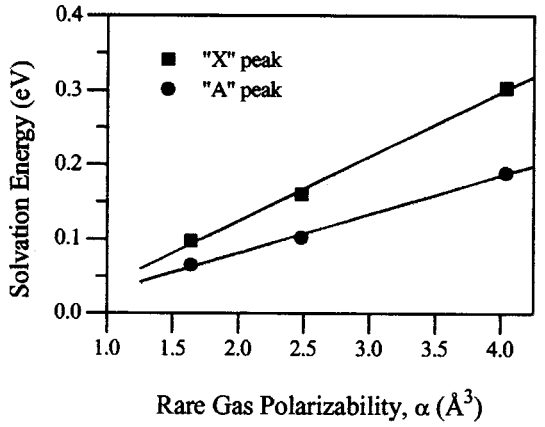


FIG. 3. Solvation energy of $O^-Rg$ complexes, Rg=Ar, Kr, and Xe, vs rare gas polarizability.

tachment from different anion states. These peaks have been labeled *X* and *A*, denoting the ground and excited anion state respectively.

Photodetachment is a vertical process that accesses the neutral potential $V_{N\cdot Rg}(R)$ at the geometry of the anion $V_{N\cdot Rg}(R=R_{e,A\cdot Rg})$. Peaks in the photoelectron spectra of weakly bound complexes (which have low-energy vibrational modes) may be broadened by unresolved Franck–Condon vibrational progressions in the neutral as well as transitions from populated anion vibrational levels. In addition, broadening may occur due to bound-free transitions to the continuum region of the neutral. The electron binding energy at peak maximum is defined as the anion vertical detachment energy (VDE) for that feature. These are reported in Table I along with the solvation energy (SE), the peak shift from the detachment energy of free $O^-$ (the atomic oxygen electron affinity), and the peak spacing between the *X* and *A* features. A schematic of the photodetachment relationships is shown in Fig. 2. With the zero of the potential energy placed at the ground state neutral separated atom limit, $V_{N\cdot Rg}(R=R_{e,A\cdot Rg})$ is positive or negative depending on whether detachment of the anion accesses the continuum or the bound portion of the neutral curve. In this way the VDE may be related to the dissociation energy of the anion complex and the electron affinity of the oxygen atom or to the dissociation energy of the neutral complex, and the adiabatic electron affinity (AEA) of the oxygen rare gas complex as follows:

$$\mathrm{VDE}=D_{0,A\cdot Rg}+\mathrm{EA_N}+V_{N\cdot Rg}(R=R_{e,A\cdot Rg}), \tag{1}$$

$$\mathrm{VDE}=D_{0,N\cdot Rg}+\mathrm{AEA}_{N\cdot Rg}+V_{N\cdot Rg}(R=R_{e,A\cdot Rg}). \tag{2}$$

Neutral complexes have broad wells with depths an order of magnitude smaller than their respective anion complexes. Under these conditions, with $D_{0,N\cdot Rg}$ and $V_{N\cdot Rg}(R=R_{e,A\cdot Rg})$ neglected in the above equations, the measured VDE is a good approximation to the adiabatic electron affinity of the neutral complex, Eq. (2), and the solvation energy, $\mathrm{SE}=\mathrm{VDE}-\mathrm{EA_N}$, is a reasonable approximation to the anion well depth, Eq. (1).

Examination of the spectra in Fig. 1 and the VDEs in Table I reveal that while the *X* and *A* features both move to progressively tighter electron binding energy with periodicity, the *X* feature does so at a greater rate (the VDEs of the *X* and *A* peaks shift by 0.206 and 0.128 eV, respectively, for Rg=Ar–Xe). In Fig. 3 a plot of VDE versus solvent polarizability demonstrates that this interaction is roughly linear for both features.

The different amount of broadening for these two features with periodicity is also readily apparent. Broadening in the *A* feature remains essentially constant for Ar, Kr, and Xe

TABLE I. VDEs of the *X* and *A* peaks in the photoelectron spectra of $O^-Rg$. The solvation energies were determined from the spectral shift the detachment energy of $O^-$, S.E.=VDE($O^-Rg$)−EA($O^-$). Peak widths were determined by fitting to Gaussians. VDE error bars are ±5 meV.

| | | VDE (eV) | S.E. (eV) | ΔVDE(*X*−*A*) (eV) | FWHM (eV) |
|---|---|---|---|---|---|
| $O^-Ar$ | *X* | 1.562 | 0.097 | 0.038 | 0.068 |
| | *A* | 1.524 | 0.059 | | 0.086 |
| $O^-Kr$ | *X* | 1.625 | 0.160 | 0.060 | 0.089 |
| | *A* | 1.565 | 0.100 | | 0.087 |
| $O^-Xe$ | *X* | 1.768 | 0.303 | 0.116 | 0.114 |
| | *A* | 1.652 | 0.187 | | 0.086 |
| $O^-N_2$ | *X* | 1.666 | 0.201 | 0.097 | 0.099 |
| | *A* | 1.569 | 0.104 | | 0.072 |

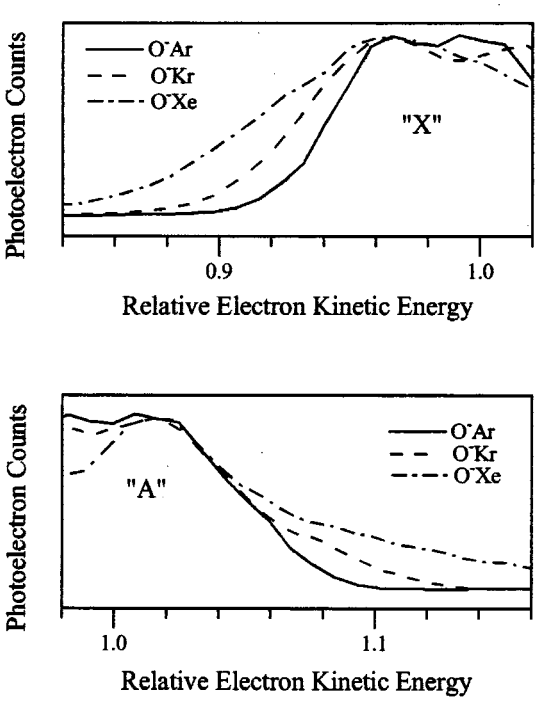


FIG. 4. The $O^-Rg$, Rg=Ar, Kr, and Xe, photoelectron spectra shifted to overlay the *X* and *A* photodetachment transitions.

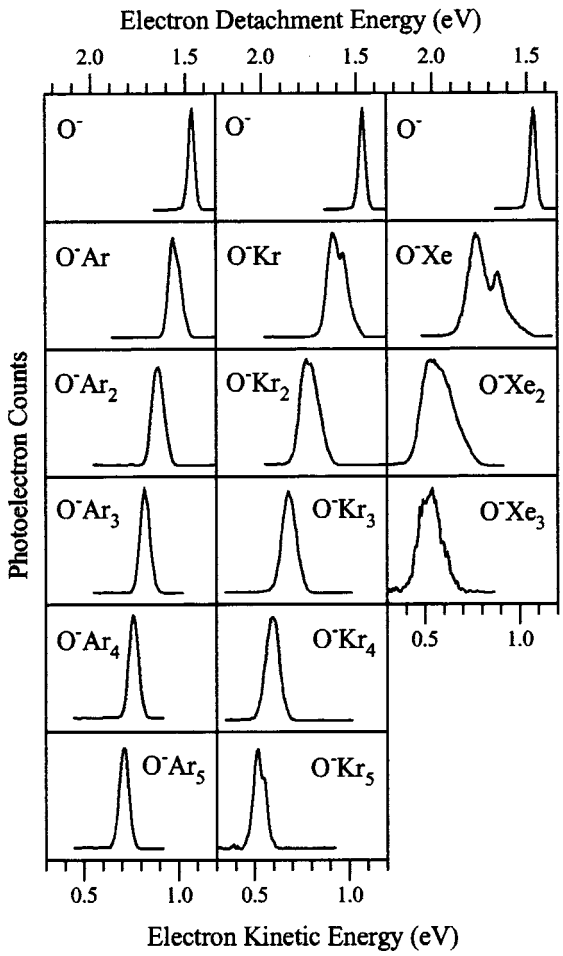


FIG. 5. Photoelectron spectra of the $O^-Rg_{n=1-5}$ cluster series, Rg=Ar, Kr, Xe.

rare gas solvent, at 0.086, 0.087, and 0.086 eV FWHM, respectively, while broadening in the *X* feature increases moderately between Ar and Kr, from 0.068 to 0.089 eV FWHM, and has a large increase to 0.114 eV FWHM for the xenon complex. In Fig. 4 the spectra have been shifted and overlaid for both the *X* and *A* feature so that the broadening may be easily compared.

In addition to the diatomic anions, the larger clusters, $O^-Xe_{n=2-3}$ and $O^-Kr_{n=2-5}$, were also produced and photodetached. Their spectra are shown in Fig. 5 along with the previously published $O^-Ar_{n=1-5}$ spectra for comparison. As expected, the VDEs increase with increasing solvation by rare gas, but in successively smaller increments. The VDEs and FWHM are reported in Table II. It is interesting that the spectral width significantly decreases after $n=2$ for all three series. After $n=2$ the peaks undergo a moderate decrease in width with increased cluster size.

In synopsis, the trends to be noticed from the data are that the strength of the interaction (the splitting between the *X* and the *A* feature) and the broadening of the *X* peak both dramatically increase with the periodicity, and hence the polarizability, of the solvent atom.

## IV. ANALYSIS AND DISCUSSION

Both dispersion and ion-induced dipole forces depend upon the polarizability of the rare gas partner, hence well depths are greatest for the xenon and shallowest for the argon complexes. For open shell species the anisotropy in the potential also increases with the interaction strength. As noted earlier, the spatial degeneracy of the atomic *P* states is removed upon interaction with the rare gas. As the interaction strength increases the perturbation of the atomic structure is magnified. In neutral oxygen rare gas complexes the dispersion interaction is weak enough that the six states associated with the $O(^3P_{2,1,0})+Rg(^1S_0)$ asymptotes span approximately the same energy difference as the three atomic oxygen spin orbit states. For example, in XeO the difference in well depths for the $^3\Pi_2$ ground state and the uppermost $^3\Sigma$ state is only 6.5 meV. In ArO this difference is only 2.9 meV. Consequently, the splitting between the ground and uppermost state in the neutral complexes are only 2.9–6.5 meV greater than the atomic oxygen $^3P_3-^3P_0$ difference of 28.1 meV, while the number of energy levels within this range has increased from three to six. At the 25 meV resolution employed here, these states would not be resolved. If the interaction strength remains relatively weak in the anion complexes, the anion state splitting should also be small. In this case, the most noticeable difference between the photoelectron spectra of the oxide anion complexes and free oxygen anion would be an overall shift to higher electron binding energy proportional to the rare gas polarizability, with some small peak broadening due to the few meV increase in level spacing in both the anion and neutral states. This is essentially the ''chromophore'' argument used with success in a great number of ion solvation studies, including the photoelectron study of $O^-Ar_{n=1-26,34}$ performed by this group.[32] However, unlike the single 37 meV FWHM peak observed in

TABLE II. Vertical detachment energies and peak widths for the cluster anion series, $O^-Ar_{n=1-5}$, $O^-Kr_{n=1-5}$, and $O^-Xe_{n=1-3}$, under cold source conditions. VDE error bars are ±5 meV.

| | $O^-Ar_n$ | | $O^-Kr_n$ | | $O^-Xe_n$ | |
|---|---|---|---|---|---|---|
| $n$ | VDE (eV) | FWHM (eV) | VDE (eV) | FWHM (eV) | VDE (eV) | FWHM (eV) |
| 1 | 1.562 | 0.069 | (1.609)[a] | (0.110)[a] | (1.752)[a] | (0.171)[a] |
| 2 | 1.648 | 0.072 | 1.753 | 0.108 | 1.985 | 0.178 |
| 3 | 1.717 | 0.061 | 1.858 | 0.087 | 2.019 | 0.138 |
| 4 | 1.778 | 0.059 | 1.945 | 0.084 | | |
| 5 | 1.828 | 0.058 | 2.019 | 0.073 | | |

[a]The "cold" spectra of the $n=1$ clusters of $O^-Kr$ and $O^-Xe$ were fit to a single asymmetric Gaussian to produce an average VDE and FWHM to facilitate comparison to the unresolved $n>2$ spectra.

the photoelectron spectrum of free $O^-$ at 25 meV resolution, the $O^-Kr$ and $O^-Xe$ spectra contain two partially resolved peaks separated by 60 and 116 meV, respectively. Since the neutral states are more closely spaced than our instrumental resolution, these peaks correspond to detachment from ground and excited states of the anion, a conclusion confirmed by the source-dependent nature of their relative intensities. The *X* and *A* peaks have been assigned to photodetachment transitions from the $^2\Sigma$ ground state and unresolved $^2\Pi_{3/2,1/2}$ excited states, respectively. Increasing the electronic temperature of the anion complexes by varying source conditions also allowed us to discern the spacing between the $O^-Ar$ states. The $O^-Ar$ $\Sigma$ and $\Pi$ states are separated by 38 meV, a spacing only slightly larger than our FWHM for photodetachment of free $O^-$. Thus, the two peaks were not apparent in the $O^-Ar$ spectra until the $\Pi$ state became significantly populated. While broadening of the chromophore peak had been noted in the previous $O^-Ar_{n=1-26,34}$ study, these spectra were acquired at the coldest possible source conditions to maximize production of argon clustering and hence transitions from the $^2\Pi$ state remained unresolved.

### A. $O^-Ar$

Examination of Fig. 4 shows only small peak broadening in the *X* and *A* peak in $O^-Ar$ relative to that of free $O^-$. This indicates that photodetachment from both the $^2\Sigma$ and the $^2\Pi$ anion states accesses the relatively flat well region of the neutral. Note, however, that neutral complexes have shallow broad potentials in the region of their wells, and the two anion states could have significantly different bond lengths and both access the neutral where the slope of the potential is small. Using Eq. (1) to take the difference in VDE between the two anion states and noting that the difference between the well depths is equal to the $^2\Sigma-^2\Pi$ anion state splitting, the peak spacing we measure is a sum of the anion $^2\Sigma-^2\Pi$ state splitting and the difference in the neutral potential energy at the two anion bond lengths,

$$\Delta VDE_{O^-Rg(^2\Sigma)\text{-}O^-Rg(^2\Pi)} = {}^2\Sigma - {}^2\Pi + V_{ORg}(R_{e,O^-Rg(^2\Sigma)}) - V_{ORg}(R_{e,O^-Rg(^2\Pi)}). \quad (3)$$

The narrowness of the *X* and *A* features in $O^-Ar$ indicates that $V_{ORg}(R_{e,O^-Rg})$ is small for detachment from both the $^2\Sigma$ and the $^2\Pi$ anion states. The difference between them is smaller still. This allows us to assign most of the peak spacing reported in Table I, $\Delta VDE = 0.038$ eV, to the anion $^2\Sigma-^2\Pi$ state splitting. Sheehy's calculation of the $O^-Ar$ potential curves finds a $^2\Sigma-^2\Pi$ splitting of 0.033 eV, consistent with the photoelectron spectrum, and bond lengths, $R_e(^2\Sigma) = 3.0$ Å and $R_e(^2\Pi) = 3.4$ Å.[35] The recent calculations of the $O^-Ar$ potential by Chalasinski and co-workers[36] are consistent with these unpublished calculations and both sets of values are included in Table III for comparison. Aquilanti's neutral curve for the OAr ground state has a well depth, $\varepsilon = 10.4$ meV at $R_e = 3.45$ Å, and crosses the zero of the potential at $\sigma = 3.05$ Å.[23] This neutral curve has an energy difference, $\Delta V_{ORg}(R_{e,O^-Rg}) = 5$ meV, between the two anion bond lengths from Ref. 35. When this is subtracted from the peak spacing in the photoelectron spectrum, Eq. (3), we find a $^2\Sigma-^2\Pi$ anion splitting of 0.033 eV, in excellent agreement with Sheehy's calculated result for this quantity. Note that the calculated $^2\Sigma$ anion bond length is close to the neutral zero of the potential and the $^2\Pi$ bond length is somewhat shorter than the neutral equilibrium bond length. The electron configuration of the oxygen anion in the $^2\Pi$ state is $p_x^1p_y^2p_z^2$, and, with a filled $O^-2p$ orbital directed toward the rare gas, is a predominantly a closed shell interaction. In contrast, the singly occupied $O^-2p$ orbital lies along the bond axis in the $^2\Sigma$ state and is a true open shell–closed shell interaction. Therefore, it is not surprising that the $^2\Pi$ anion state has a longer bond than the $^2\Sigma$ anion state. What might seem counter-intuitive is that the $O^-Ar$ $^2\Pi$ bond length is only a little shorter than the neutral OAr bond

TABLE III. Potential parameters for $O^-Rg$, Rg=Ar,Kr,Xe.

| | $^2\Sigma$ | | $^2\Pi$ | |
|---|---|---|---|---|
| $O^-Rg$ | $D_0$ (eV) | $r_e$ (Å) | $D_0$ (meV) | $r_e$ (Å) |
| $O^-Ar$ | 97 | | 64 | |
| ( )[a] | (100) | (3.0) | (67) | (3.38) |
| [ ][b] | [97.68] | [3.013] | [66.03] | [3.408] |
| $O^-Kr$ | 147–160 | 3.05–3.16 | 113 | 3.50 |
| [ ][b] | [158.43] | [2.963] | [114.43] | [3.322] |
| $O^-Xe$ | 238–303 | 2.98–3.26 | 205 | 3.61 |

[a]Results from M. Fajardo's preliminary calculations (Ref. 35).
[b]Calculated results for $O^-Ar$ and $O^-Kr$ (Ref. 38).
[c]All other numbers determined from the photoelectron data for the anion complexes reported here using Aquilanti's (Ref. 23) scattering data for the neutral ground state $|2,2\rangle$ potential curves as described in the interpretation section.

though the ion-induced dipole interaction is substantially stronger than the dispersion interaction. With a solvation energy of 0.059 eV the $O^-Ar\,^2\Pi$ state has a dissociation energy approximately six times that of the neutral; however, the size of the atomic oxygen anion is significantly larger than the neutral oxygen atom. For the $O^-Ar\,^2\Pi$ state the strength of the ion induced dipole versus the dispersion interaction is just sufficient to counter the increased size of the $O^-$ anion. These competing effects have been noted in ZEKE studies of Ar, Kr, and Xe complexes of $Cl^-$, $Br^-$, and $I^-$,[3,6] where the closed shell anion–rare gas interaction is similar to the closed shell nature of the $^2\Pi$ state in $O^-Ar$. These investigations find that the difference in bond length between anion and ground state neutral is very small, for all of the halogen anion rare gas systems studied, though the anion complexes have significantly deeper wells.

The good agreement between the measured peak spacing and the calculated splitting indicate that Sheehy's calculations give a good account of the anisotropy of the interaction of $O^-$ with argon, which preferentially shortens the bond and deepens the well of the $^2\Sigma$ ground state. In the discussion which follows, conclusions will be drawn by comparing the $O^-Kr$ and $O^-Xe$ spectra to the $O^-Ar$ photoelectron spectrum with reference to the potential curves of $O^-Ar$[35] and ORg.[23]

### B. $^2\Pi$ states of $O^-Kr$ and $O^-Xe$

In the spectra of $O^-Kr$ and $O^-Xe$, the *A* peak remains as narrow as that observed in the $O^-Ar$ spectrum (note that broadening at the base is due to vibrational excitation of the anion). Since the manifold of neutral ORg states span an energy range close to that of the atomic oxygen spin orbit states, broadening in significant excess to that observed in the photoelectron spectrum of free $O^-$ should be due to unresolved weak mode Franck–Condon and/or bound-free transitions. The small peak broadening for photodetachment from the $^2\Pi$ states of $O^-Kr$ and $O^-Xe$, similar to that observed in the spectrum of $O^-Ar$, indicates that they each have a similar relationship to their respective neutral potentials, i.e., the anion bond lengths are close to the neutral equilibrium bond length. The small broadening observed in photoelectron spectra for the $^2\Pi$ states of $O^-Kr$ and $O^-Xe$ is, as in $O^-Ar$, consistent with the ZEKE results for the halogen anion rare gas closed shell interaction.

When photodetachment accesses the bound region of the neutral, as is the case here, $V_N(R)\leqslant 0$ in Eq. (1) and the solvation energy is less than the dissociation energy of the anion state. Therefore the solvation energy we find is a lower bound to the dissociation energy of the $^2\Pi$ states, 0.100 and 0.187 eV in $O^-Kr$ and $O^-Xe$, respectively. Using information for the ground state OKr potential from Ref. 23 ($\varepsilon = 13.1$ meV, $R_e = 3.57$ Å, and $\sigma = 3.16$ Å), and assuming a proportionally similar relationship between anion and neutral bond length as found in $O^-Ar$, gives the $O^-Kr\,^2\Pi$ state a bond length of 3.5 Å. At this bond length neutral OKr has a potential energy of $-13$ meV, found using Eqs. (4), (7), and (8) from Ref. 23. Subtracting $V_N(R) = -13$ meV from the solvation energy for this photodetachment peak gives a dissociation energy of 0.113 eV for the $O^-Kr\,^2\Pi$ state, Eq. (1). This result for the $O^-Kr\,^2\Pi$ state is consistent with the calculations of Chalasinski and co-workers who find a dissociation energy of 0.109 eV and a bond length of 3.359 Å for the $O^-Kr\,^2\Pi$ state. Similarly, using Aquilanti's neutral curve for the ground state OXe potential ($\varepsilon = 17.30$ meV, $R_e$ = of 3.69 Å, and $\sigma = 3.26$ Å) gives the $O^-Xe\,^2\Pi$ state a bond length of 3.61 Å. At this bond length neutral OXe has a potential energy of $-17$ meV that when subtracted from the solvation energy gives a dissociation energy of 0.204 eV.

### C. $^2\Sigma$ states of $O^-Kr$ and $O^-Xe$

As noted, calculations consistent with our data find a bond length for the $O^-Ar\,^2\Sigma$ state close to the zero of the potential of the OAr neutral. Because the *X* feature in $O^-Kr$ is broader than this feature in $O^-Ar$, and broader still in $O^-Xe$, the bond length of the $^2\Sigma$ states in these complexes should be shorter relative to their respective neutrals than that found in the $O^-Ar\,^2\Sigma$ state. Thus, the zero of the potential of the respective neutrals are upper bounds for the $^2\Sigma$ anion bond lengths, $R_e(O^-Kr\,^2\Sigma)\leqslant\sigma(OKr) = 3.16$ Å and $R_e(O^-Xe\,^2\Sigma)\leqslant\sigma(OXe) = 3.26$ Å. Photodetachment from anions with bond lengths shorter than the neutral zero of the potential accesses the repulsive wall of the neutral. Consequently, $V_N(R)\geqslant 0$ in Eq. (1) and the solvation energy of the peak is greater than the dissociation energy of the anion state. Therefore the upper bound to the dissociation energy of the $^2\Sigma$ state is 0.160 eV in $O^-Kr$ and 0.303 eV in $O^-Xe$.

A lower limit for the $^2\Sigma$ bond lengths and dissociation energies can be determined from the vertical detachment energies reported here by noting that the $^2\Sigma - ^2\Pi$ splitting is expected to get larger as the polarizability of the rare gas increases. Thus the 0.33 eV $O^-Ar\,^2\Sigma - ^2\Pi$ splitting is a lower limit for the $O^-Kr$ and $O^-Xe$ $^2\Sigma$-$^2\Pi$ splitting. Adding this to the $^2\Pi$ dissociation energies gives a lower limit for the $^2\Sigma$ dissociation energies of 0.146 and 0.238 eV in $O^-Kr$ and $O^-Xe$, respectively. The difference between the solvation energy for the *X* feature and the lower limit of the $^2\Sigma$ dissociation energy is the upper limit to the neutral potential accessed by photodetachment of the anion [$SE - D_{0,ARg} = V_N(R)$ from Eq. (1)]. The maximum height of the repulsive wall of the neutral that may be accessed by photodetachment corresponds to the lower limit for the anion bond length and is $0.160 - 0.146 = 0.014$ eV and $0.303 - 0.238 = 0.067$ meV for detachment from the $^2\Sigma$ states of $O^-Kr$ and $O^-Xe$, respectively. Using equations for the ground state neutral potentials from Ref. 23 the minimum bond length are found to be $R_e(O^-Kr\,^2\Sigma) \geqslant = 3.05$ Å and $R_e(O^-Xe\,^2\Sigma) \geqslant = 2.98$ Å.

In summary, the $O^-Kr\,^2\Sigma$ state is found to have an equilibrium bond length, 3.05 Å $\leqslant R_e \leqslant$ 3.16 Å, and dissociation energy, 0.146 eV $\leqslant D_o \leqslant$ 0.160 eV. The $^2\Sigma$ state of $O^-Xe$ is found to have an equilibrium bond length, 2.98 Å $\leqslant R_e \leqslant$ 3.26 Å, and a dissociation energy, 0.238 eV $\leqslant D_o \leqslant$ 0.303 eV. Note that while the value of the neutral potential accessed by photodetachment was derived from the vertical detachment energies reported here, the determination of the

bond lengths at that potential depended upon the accuracy of the repulsive wall of the neutrals reported in Ref. 23. The determination of the anion dissociation energies was derived primarily from the vertical detachment energies.

### D. Nature of the $^2\Sigma$ and $^2\Pi$ interaction

Just as an examination of neutral versus anion bond lengths for a given rare gas complex requires consideration of the competing effects of increased anion size versus increased interaction strength, a consideration of bond lengths across a periodic rare gas series (whether anionic or neutral) must account for both the increased size and the increased polarizability of the rare gas partner. In neutral closed shell systems, where the interaction strength is relatively low, the increased polarizability of the larger rare gases is not sufficient to offset the increase in atomic radii and the net effect is that the bond length increases with periodicity.[42] In open shell systems the anisotropy of the interaction makes these relationships less straightforward.

Neutral fluorine and chlorine rare gas complexes are isoelectronic with $O^-Rg$ and have been well characterized by scattering studies over the periodic series from He to Xe.[26,29] In both the fluorine and chlorine systems the $^2\Pi$ bond lengths increase with rare gas periodicity, behavior similar to that observed in the rare gas–rare gas complexes. In contrast, bond length trends of the $^2\Sigma$ states, where the bonding has a strong anisotropic component, vary from one halogen system to another. In the fluorine–rare gas series, where the anisotropy is very strong, bond lengths of the $^2\Sigma$ states decrease over the periodic series from He to Xe, behavior counter to that observed in the $^2\Pi$ states and in closed shell systems. In the chlorine–rare gas system, however, where the anisotropy is weaker, bond lengths of the $^2\Sigma$ states increase from helium to argon and have a small decrease between argon and krypton, followed by a substantial drop in bond length between the krypton and xenon complexes.

The anisotropy in the halogen rare gas systems that leads to a deeper well and shorter bond for the $^2\Sigma$ states has been related to two phenomena: the formation of an incipient covalent bond due to the one electron contact with the rare gas, and ionic character due to the mixing of relatively low lying ionic potentials of $^2\Sigma$ symmetry. For the halogen complexes stabilization by charge transfer is a significant factor in the increased stability of the $^2\Sigma$ state due to the large positive electron affinity of the halogen atom. This is particularly evident in the FXe potential. The van der Waals interaction strength approaches that of the fluorine atom spin orbit interaction and the two states straddle the transition between a separated atom Hund's case *c* and a molecular Hund's case *a* description.[26] In the case of the $FXe\,^2\Pi$ states the interaction remains weak enough that the well region of the potential remains in the Hund's case *c* region. However, due to the increased stabilization due to charge transfer the $FXe\,^2\Sigma$ state has a dramatic increase in well depth relative to the $^2\Pi$ states (161.8 versus 6.8 meV) and falls well within a Hund's case *a* description.[26]

Though the dissociation energies of the $O^-\,Rg\,^2\Sigma$ and $^2\Pi$ anion states are significantly greater than in F–Rg, as is expected for an ion-induced dipole interaction, the peak spacing in $O^-Rg$ is smaller than the 155 meV $FXe\,^2\Sigma-^2\Pi$ splitting ($\Delta VDE = 116$ meV is an upper limit to the $O^-Xe\,^2\Sigma-^2\Pi$ splitting and the width of the *X* peak indicates that it is significantly smaller than this). Therefore, we can conclude that while the interaction is stronger in $O^-Rg$ than F–Rg, the degree of anisotropy in the potential is smaller. The bond length trend also supports this conclusion. As discussed, the rare gas complexes of fluorine and chlorine show different degrees of the same general phenomena. Bond lengths of the $^2\Pi$ states, where the interaction is mostly spherical, increase with the periodicity of the rare gas for both halogen systems. The bond lengths of the $^2\Sigma$ states, which are sensitive to anisotropy in the potential, decrease with periodicity over the entire He–Xe series for fluorine, but only from Ar–Xe for chlorine, with the drop between the krypton and xenon complexes being half an angstrom or more. For the complexes of rare gas with the "halogenlike" oxygen anion this effect is weaker still. The bond lengths for the $^2\Pi$ states increase with periodicity, $R_e(O^-Ar,^2\Pi) = 3.4$ Å, $R_e(O^-Kr,^2\Pi) = 3.5$ Å, and $R_e(O^-Xe,^2\Pi) = 3.61$ Å, as expected for a mostly spherical interaction. The bond lengths of the $^2\Sigma$ states, however, remain relatively constant or somewhat increasing over the range of Ar to Xe, $R_e(O^-Ar,^2\Sigma) = 3.0$ Å, $R_e(O^-Kr,^2\Sigma) = 3.0–3.11$ Å, and $R_e(O^-Xe,^2\Sigma) = 2.98–3.26$ Å. At first this result, increasing bond length for the $^2\Sigma$ states with rare gas periodicity, seems counter-intuitive. For the neutral halogen–rare gas complexes the effect of anisotropy in the potential is more apparent when the intermolecular interaction is stronger (i.e., F–Rg versus Cl–Rg). So, one might expect that the stronger ion-induced dipole interactions would show greater effects than their isoelectronic-induced counterparts. However, in this case, the weaker anisotropy observed in $O^-Rg$ is a consequence of the strong nature of the ion-induced dipole interaction. The strength of the ion-induced dipole interaction is such that both the $^2\Sigma$ and $^2\Pi$ states fall under a Hund's case *a* description and because the $O^{2-}$ atomic anion is not a stable gas phase species the potential curves for these ionic states lie at too high of an energy to stabilize the $O^-Rg\ ^2\Sigma$ state to an appreciable degree. The effect of anisotropy in the potential of $O^-Rg$ is manifested predominantly by the difference in stability for one and two electron contact rather than a difference in ionic versus covalent or molecular versus separated atom nature. This system therefore is an ideal case where the difference in intermolecular interaction due to open shell versus closed shell nature may be examined without a corresponding charge transfer contribution.

### E. $O^-Rg_{n=1-5}$

In the diatomic $O^-Rg$ clusters, the solvation energies of the *X* and *A* peaks approximate the interaction strength of the $^2\Sigma$ and $^2\Pi$ anion states and hence the interaction strength of the rare gas with the open $O^-2p_z^1$ versus the closed $O^-2p_x^2$ and $2p_y^2$ atomic orbitals. The *sequential* solvation energy in cluster series is simply the difference in VDE for adjacent clusters and reflects the stabilization of the negative charge by additional solvent rare gas as well as the attractive inter-

actions between solvent molecules. For small cluster ions where the charge is largely exposed and where the solvent interaction with the ion is an order of magnitude greater than the solvent–solvent interaction, electron stabilization will be the dominant contribution to cluster stability. Therefore, if the sequential solvation energy for adjacent clusters is significantly larger than the solvation energy of the $^2\Pi$ state in the dimer, then it is reasonable to conclude that the additional solvent rare gas molecule is bonding with the open $2p_z$ orbital. The solvation energy for the *A* peak in $O^-Ar$ is 0.059 eV. The sequential solvation energy for the $O^-Ar_2$ cluster is 0.086 eV. Similarly, the solvation energy for the *A* peak in $O^-Kr$ is 0.100 eV while the sequential solvation energy for the $O^-Kr_2$ cluster is 0.131 eV from the $^2\Sigma$ state. In both cases the solvation energy upon the addition of a second rare gas is ~0.030 eV greater than the $^2\Pi$ closed shell interaction in the diatomic. When one additionally considers that the effect of an interaction diminishes with increasing cluster size as the charge interacts with a greater number of solvent molecules, it is clear that a closed shell interaction cannot be responsible for the large sequential solvation energy observed for the $n=2$ clusters. Addition of a second rare gas atom to the $2p_z^1$ orbital of the $^2\Sigma$ and the $^2\Pi$ diatomic states leads to two cluster geometries in the $O^-Rg_2$ trimer. The $O^-2p_z^1$ orbital is bonded to the rare gas in the $^2\Sigma$ diatomic state, therefore the addition of a second rare gas to the $O^-2p_z^1$ orbital leads to an open shell linear $O^-Rg_2$ structure. The $O^-2p_z^1$ orbital is nonbonding in the $^2\Pi$ diatomic state (the rare gas bonds to the $2p_x^2$, or $2p_y^2$ atomic orbitals). The addition of a rare gas to the $O^-2p_z^1$ orbital of the $^2\Pi$ diatomic leads to an open shell perpendicular geometry in the subsequent cluster trimer. Note that the open shell perpendicular structure can also be formed by addition of a rare gas atom to a filled orbital of the $^2\Sigma$ diatomic state. The linear and perpendicular trimer geometries differ from each other in much the same way as the diatomic $^2\Sigma$ and $^2\Pi$ states from which they stem, and can be expected to have a similar state splitting, resulting in a broad photodetachment peak. Because the photodetachment peak is broad and unresolved in the trimers, we cannot preclude the presence of unresolved low-intensity transitions from the other two possible geometries (linear and perpendicular across both closed shell orbitals). However, the open shell geometries should account for the bulk of the peak intensity. Consider now the $O^-Rg_3$ tetramer. As in $O^-Rg_2$, there are four nonequivalent ways to place three rare gas atoms about the $O^-$ sub-ion. However, if we consider that, during cluster growth $O^-Rg_3$ clusters will be formed from the population of $O^-Rg_2$ clusters, which are predominantly open shell linear and perpendicular geometries, the addition of a third rare gas to the open shell linear structure produces only one geometry, a planar arrangement with two rare gases interacting with the $O^-2p_z^1$ orbital and one interacting with a $O^-2p_x^2$ or $2p_y^2$ orbital. This planar arrangement would also be the most stable result of addition of a third rare gas atom to the open shell perpendicular trimer by minimizing electron repulsion. In addition, evaporative cooling will remove less stable cluster geometries from the expansion more quickly. The conclusion that the $O^-Rg_3$ clusters in our expansion are predominantly the planar structure is supported by the drop in peak width for the $n=3$ clusters, after which the FWHM continues to decrease but at a moderate pace.

## V. CONCLUSIONS

We have recorded the 488 nm photoelectron spectra of $O^-Rg$, where Rg=Ar, Kr, Xe, and $O^-N_2$, as well as the larger clusters $O^-Kr_{n=1-5}$ and $O^-Xe_{n=1-5}$. Unlike the single unresolved peak observed in the spectrum of free $O^-$ at 25 meV resolution, the photoelectron spectra of the oxide anion rare gas diatomics have two distinct photoelectron peaks. The relative intensities of these peaks were found to vary greatly with source conditions and hence were assigned to the ground and low-lying excited states of the anion, the $^2\Sigma$ and $^2\Pi$ states, respectively. These states result from the isotropic interaction between the open shell $O^-(^2P_{3/2,1/2})$ sub-ion and the rare gas that lifts the degeneracy of the atomic oxygen $2p$ orbitals. We find solvation energies and peak splittings from the vertical detachment energies we measure, which are reasonable approximations to the dissociation energies and state splittings for the $^2\Sigma$ and $^2\Pi$ anion states. By examining the spectral broadening evident in the photoelectron spectra and using information on the neutral curves accessed during photodetachment we are able to improve upon these numbers. These results are compared to calculated results which are found to be consistent with experiment. The vertical detachment energies of both features move to progressively tighter binding energy with periodicity, the peak assigned to the $^2\Sigma$ state doing so at a much greater rate. This is related to the open shell nature of this state which reduces electron–electron repulsion.

## ACKNOWLEDGMENTS

The authors thank Jeffrey Sheehy and Mario Fajardo for sharing unpublished results with us early in the experiment. We would also like to thank Alexei Buchachenko, Maria Szczęśniak, and Grzegorz Chalasiński for sharing and discussing their theoretical results with us. We gratefully acknowledge the support of the National Science Foundation under Grant Nos. CHE-9007445 and CHE-9816229.

[1] C. Crépin-Gilbert and A. Tramer, Int. Rev. Phys. Chem. **18**, 485 (1999).
[2] M. C. Heaven, Annu. Rev. Phys. Chem. **43**, 283 (1992).
[3] Y. Zhao, I. Yourshaw, G. Reiser, C. C. Arnold, and D. M. Neumark, J. Chem. Phys. **101**, 6538 (1994).
[4] I. Yourshaw, T. Lenzer, G. Reiser, and D. M. Neumark, J. Chem. Phys. **109**, 5247 (1998).
[5] T. Lenzer, M. R. Furlanetto, K. R. Asmis, and D. M. Neumark, J. Chem. Phys. **109**, 10754 (1998).
[6] T. Lenzer, I. Yourshaw, M. R. Furlanetto, G. Reiser, and D. M. Neumark, J. Chem. Phys. **110**, 9578 (1999).
[7] I. Yourshaw, Y. Zhao, and D. M. Neumark, J. Chem. Phys. **105**, 351 (1996).
[8] T. Lenzer, M. R. Furlanetto, N. L. Pivonka, and D. M. Neumark, J. Chem. Phys. **110**, 6714 (1999).
[9] F. Breyer, P. Frey, and H. Hotop, Z. Phys. A **286**, 133 (1978).
[10] D. M. Neumark, K. R. Lykke, T. Andersen, and W. C. Lineberger, Phys. Rev. A **32**, 1890 (1985).
[11] C. Blondel, Phys. Scr., T **T58**, 31 (1995).
[12] C. Kenty, J. O. Aicher, E. B. Noel, A. Poritsky, and V. Paolino, Phys. Rev. **69**, 36 (1946).

[13] C. D. Cooper, G. C. Cobb, and E. L. Tolnas, J. Mol. Spectrosc. **7**, 223 (1961).
[14] H. T. Powell, J. R. Murray, and C. K. Rhodes, Appl. Phys. Lett. **25**, 730 (1974).
[15] D. C. Lorents and D. L. Huestis, in *Lecture Notes in Physics Vol. 43; Laser Spectroscopy*, edited by S. Haroche (Springer, Berlin, 1975), p. 100.
[16] G. C. Tisone, J. Chem. Phys. **60**, 3716 (1974).
[17] N. G. Basov, V. S. Zuev, L. D. Mikheev, V. K. Orlov, I. V. Pogorel'skii, and A. V. Yalovoi, Sov. J. Quantum Electron. **6**, 505 (1976).
[18] J. Goodman, J. C. Tully, V. E. Bondybey, and L. E. Brus, J. Chem. Phys. **66**, 4802 (1977).
[19] T. H. Dunning, Jr. and P. J. Hay, J. Chem. Phys. **66**, 3767 (1977).
[20] J. S. Cohen, W. R. Wadt, and P. J. Hay, J. Chem. Phys. **71**, 2955 (1979).
[21] S. R. Langhoff, J. Chem. Phys. **73**, 2379 (1980).
[22] R. J. Donovan and D. Husain, Chem. Rev. **70**, 489 (1970).
[23] V. Aquilanti, R. Candori, and F. Pirani, J. Chem. Phys. **89**, 6157 (1988).
[24] V. Aquilanti, F. Pirani, and F. Vecchiocattivi, in *Structure and Dynamics of Weakly Bound Molecular Complexes*, edited by A. Weber (Plenum, New York, 1987), p. 423.
[25] V. Aquilanti, R. Candori, L. Mariani, F. Pirani, and G. Liuti, J. Phys. Chem. **93**, 130 (1989).
[26] V. Aquilanti, E. Luzzatti, F. Pirani, and G. G. Volpi, J. Chem. Phys. **89**, 6165 (1988).
[27] V. Aquilanti, G. Liuti, F. Pirani, and F. Vecchiocattivi, J. Chem. Soc., Faraday Trans. 2 **85**, 955 (1989).
[28] V. Aquilanti, D. Cappelletti, V. Lorent, E. Luzzatti, and F. Pirani, Chem. Phys. Lett. **192**, 153 (1992).
[29] V. Aquilanti, D. Cappelletti, V. Lorent, E. Luzzatti, and F. Pirani, J. Phys. Chem. **97**, 2063 (1993).
[30] M. McFarland, D. L. Albritton, F. C. Fehsenfeld, E. E. Ferguson, and A. L. Schmeltekopf, J. Chem. Phys. **59**, 6610 (1973); H. W. Ellis, R. Y. Pai, E. W. McDaniel, E. A. Mason, and L. A. Viehland, At. Data Nucl. Data Tables **17**, 177 (1976).
[31] A. A. Viggiano, R. A. Morris, and E. A. Mason, J. Chem. Phys. **98**, 6483 (1993).
[32] S. T. Arnold, J. H. Hendricks, and K. H. Bowen, J. Chem. Phys. **102**, 39 (1995).
[33] S. L. Lin and J. N. Bardsley, J. Chem. Phys. **66**, 435 (1977).
[34] V. L. Bychov, Teplofiz. Vys. Temp. **20**, 765 (1982), in Russian.
[35] M. Fajardo and Jeffrey Sheehy (private communications).
[36] A. A. Buchachenko, J. Jakowski, G. Chalasiński, M. M. Szczęśniak, and S. M. Cybulski, J. Chem. Phys. **112**, 5852 (2000).
[37] G. Chalasiński and M. M. Szczęśniak, Chem. Rev. **100**, 4227 (2000).
[38] A. A. Buchachenko, M. M. Szczęśniak, Jacek Klos, and G. Chalasiński, J. Chem. Phys. **117**, 2629 (2002), following paper.
[39] S. T. Arnold, J. G. Eaton, D. Patel-Misra, H. W. Sarkas, and K. H. Bowen, in *Ion and Cluster Ion Spectroscopy and Structure*, edited by J. P. Maier (Elsevier, Amsterdam, 1987), p. 93.
[40] J. V. Coe, J. T. Snodgrass, C. B. Freidhoff, K. M. McHugh, and K. H. Bowen, J. Chem. Phys. **84**, 618 (1986).
[41] J. V. Coe, J. T. Snodgrass, C. B. Freidhoff, K. M. McHugh, and K. H. Bowen, J. Chem. Phys. **87**, 4302 (1987).
[42] R. A. Aziz, in *Inert Gases*, edited by M. L. Klein (Springer, Berlin, 1984), p. 5.